nature physics

LETTERS

https://doi.org/10.1038/s41567-018-0387-2

Evidence of a gate-tunable Mott insulator in a trilayer graphene moiré superlattice

Guorui Chen[1,2,3], Lili Jiang[1], Shuang Wu[4], Bosai Lyu[3,5], Hongyuan Li[3,5], Bheema Lingam Chittari[6], Kenji Watanabe[7], Takashi Taniguchi[7], Zhiwen Shi[3,5], Jeil Jung[6], Yuanbo Zhang[2,3,8]* and Feng Wang[1,9,10]*

The Mott insulator is a central concept in strongly correlated physics and manifests when the repulsive Coulomb interaction between electrons dominates over their kinetic energy[1,2]. Doping additional carriers into a Mott insulator can give rise to other correlated phenomena such as unusual magnetism and even high-temperature superconductivity[2,3]. A tunable Mott insulator, where the competition between the Coulomb interaction and the kinetic energy can be varied in situ, can provide an invaluable model system for the study of Mott physics. Here we report the possible realization of such a tunable Mott insulator in a trilayer graphene heterostructure with a moiré superlattice. The combination of the cubic energy dispersion in ABC-stacked trilayer graphene[4–8] and the narrow electronic minibands induced by the moiré potential[9–15] leads to the observation of insulating states at the predicted band fillings for the Mott insulator. Moreover, the insulating states in the heterostructure can be tuned: the bandgap can be modulated by a vertical electrical field, and at the same time the electron doping can be modified by a gate to fill the band from one insulating state to another. This opens up exciting opportunities to explore strongly correlated phenomena in two-dimensional moiré superlattice heterostructures.

Atomically thin two-dimensional (2D) materials with wide-ranging properties can be grown separately and then stacked together to form a new class of materials—van der Waals-bonded heterostructures—in which each layer can be engineered separately[16]. In addition, convenient control of individual layered materials may be achieved through electrostatic gating and interlayer coupling. Such van der Waals heterostructures offer the possibility to design new material systems that were not possible in the past. Fascinating physics has already been observed in different van der Waals heterostructures, such as mini-Dirac cones and the Hofstadter's butterfly pattern in graphene/hBN heterostructures[9–12,17,18], direct to indirect bandgap transitions in bilayer MoS_2 (refs. [19,20]) and interlayer exciton states in $MoSe_2/WSe_2$ heterostructures[21,22]. So far, these new phenomena in van der Waals heterostructures are limited to weakly interacting electrons. Strongly correlated physics can also emerge in suitably designed van der Waals heterostructures where the Coulomb potential dominates over the kinetic energy of band electrons. A quintessential example of correlated physics is the Mott insulator, which features an insulating state in a partially filled electronic band, usually at the density of one electron per lattice site. Previously, a 1D Mott insulator was observed in suspended single-walled carbon nanotubes due to the enhanced Coulomb interactions in lower dimensions. Here, we design an ABC-stacked trilayer graphene (ABC-TLG) and hexagonal boron nitride (hBN) heterostructure with a large moiré superlattice, and find strong evidence for a tunable 2D Mott insulator, where the Mott gap can be modulated in situ by a vertical electrical field. In addition, the electron doping can be continuously tuned via gating to fill the electronic band from one Mott insulating state to another, which is impossible to achieve for Mott insulators based on bulk natural crystals.

Graphene/hBN heterostructures offer a powerful platform to explore novel quantum phenomena due to the excellent sample quality and tunable physical properties[23] of graphene, as well as the existence of a periodic moiré superlattice[10–12]. In monolayer graphene, the massless electrons[24,25] feature a large kinetic energy, resulting in moiré minibands with rather wide energy bandwidths. Consequently, the electron–electron interaction effect is negligible for a monolayer graphene/hBN superlattice. In contrast, ABC-TLG exhibits a very flat cubic band at the K point in the first Brillouin zone[4–8]. Such a flat band gives rise to strong electron correlations and a spontaneously broken symmetry state in suspended ABC-TLG[6,26]. The addition of a moiré superlattice with a period of $L_M = 15$ nm in a zero-twist ABC-TLG/hBN heterostructure creates narrow minibands that are well separated from each other. The lowest minibands have a bandwidth of ~10 meV, which is significantly smaller than the on-site Coulomb repulsion energy of $\frac{e^2}{4\pi\varepsilon_0\varepsilon L_M} \approx 25$ meV if we use the hBN dielectric constant of $\varepsilon = 4$. In this Letter, we argue that the dominating Coulomb potential leads to prominent Mott insulating states with one hole per moiré superlattice site in the ABC-TLG/hBN heterostructure (Fig. 1a), which corresponds to 1/4 filling of the miniband due to the spin and valley degeneracy of electrons in graphene. Mott insulating states are also observed at 1/2 filling with two holes per superlattice site and at several other fractional fillings of the minibands. In addition, the band structure of the ABC-TLG can be controlled through electrostatic gating, leading to a field-tunable Mott insulator in the heterostructure.

Few-layer graphene samples were mechanically exfoliated onto a Si wafer covered with 285-nm-thick SiO_2, and the layer

[1]Department of Physics, University of California at Berkeley, Berkeley, CA, USA. [2]State Key Laboratory of Surface Physics and Department of Physics, Fudan University, Shanghai, China. [3]Collaborative Innovation Center of Advanced Microstructures, Nanjing, China. [4]Department of Electrical Engineering and Computer Sciences, University of California, Berkeley, CA, USA. [5]Key Laboratory of Artificial Structures and Quantum Control (Ministry of Education), School of Physics and Astronomy, Shanghai Jiao Tong University, Shanghai, China. [6]Department of Physics, University of Seoul, Seoul, Korea. [7]National Institute for Materials Science, Tsukuba, Japan. [8]Institute for Nanoelectronic Devices and Quantum Computing, Fudan University, Shanghai, China. [9]Materials Science Division, Lawrence Berkeley National Laboratory, Berkeley, CA, USA. [10]Kavli Energy NanoSciences Institute at the University of California, Berkeley and the Lawrence Berkeley National Laboratory, Berkeley, CA, USA. *e-mail: zhyb@fudan.edu.cn; fengwang76@berkeley.edu

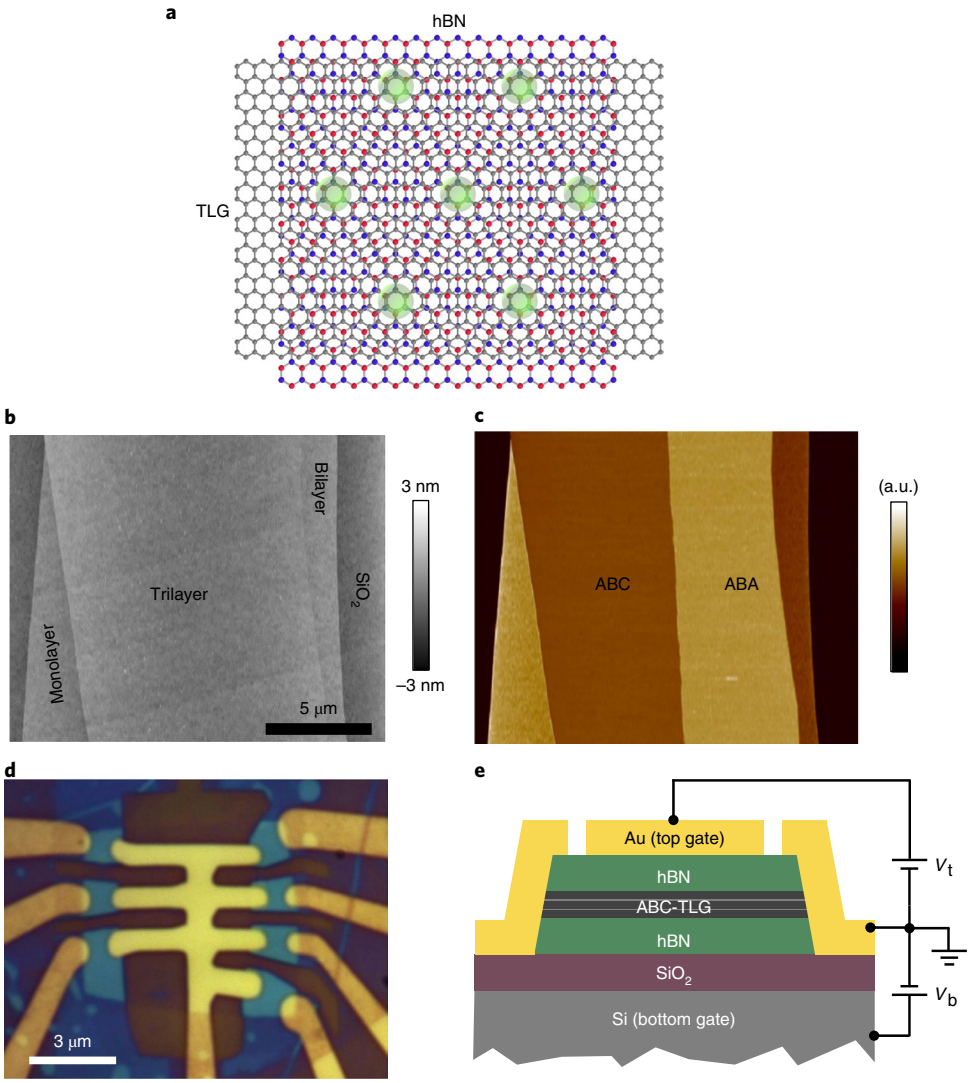

Fig. 1 | ABC-TLG/hBN moiré superlattice and dual gate FET. a, Schematic of ABC-TLG/hBN moiré superlattice. Only atoms of the top hBN layer and the bottom graphene layer are shown for image clarity. In the Mott insulating state at 1/4 filling, each electron (or hole) occupies one superlattice site and they are separated by the dominating Coulomb repulsion. **b**, Atomic force microscopy topography image of an exfoliated graphene with monolayer, bilayer and trilayer segments on a SiO_2/Si substrate. **c**, Corresponding near-field infrared nanoscopy image in which a large ABC domain exists. **d**, Optical micrograph of dual-gated ABC-TLG encapsulated by hBN. The sample is etched into a Hall bar for four-probe measurements and contacted by Cr/Pd/Au through the exposed edges. **e**, Schematic cross-sectional view of the device shown in **d**. The Au bar and doped Si served as top and bottom gate, respectively.

thickness was determined through optical contrast measurements. We used near-field infrared nanoscopy to identify ABC-TLG because it allows direct imaging of ABC and ABA regions with nanometre spatial resolution[27]. Figure 1b presents a topography image of exfoliated graphene with monolayer, bilayer and trilayer segments on a SiO_2/Si substrate using atomic force microscopy, and Fig. 1c shows the corresponding near-field nanoscopy image. The ABA and ABC regions of the TLG segment exhibit very different contrasts in the near-field nanoscopy image due to their different electronic bandstructures and infrared responses[27]. We isolated the large ABC-TLG region by cutting the sample in situ with the tip of the atomic force microscope, and created the hBN/ABC-TLG/hBN heterostructure by stacking different layers using a dry transfer method[23]. We identified the crystal orientation of the ABC-TLG and hBN using the crystalline edges of the flakes and manually aligned the ABC-TLG lattice with the hBN flake during the transfer process. The device was then etched into a Hall bar structure using standard electron-beam lithography. The ABC-TLG was contacted through 1D edge contacts with Cr/Pd/Au electrodes. A metal top electrode was deposited to form a dual-gate device where the ABC-TLG/hBN heterostructures could be gated by both the top metal electrode and the bottom silicon substrate. This dual-gate configuration allowed us to independently control the carrier concentration and bandgap of the ABC-TLG[28]. Figure 1d presents an optical image of a fabricated device, and Fig. 1e shows a schematic cross-sectional view of the device. We found that the ABC trilayers often converted into ABA trilayers after the fabrication process, and only a small fraction retained the original stacking order. We confirmed the ABC stacking order of the TLG after the fabrication process by characterizing its gate-dependent resistivity and Landau level fan diagram in magnetic fields (see Supplementary Section I for details).

The ABC-TLG/hBN heterostructures can form moiré superlattices with different lattice periods. The moiré superlattice effect is strongest for zero-twist graphene and hBN layers, which have the longest moiré period of $L_M = 15$ nm. A key signature of the moiré superlattice is provided by the new resistance peaks that emerge

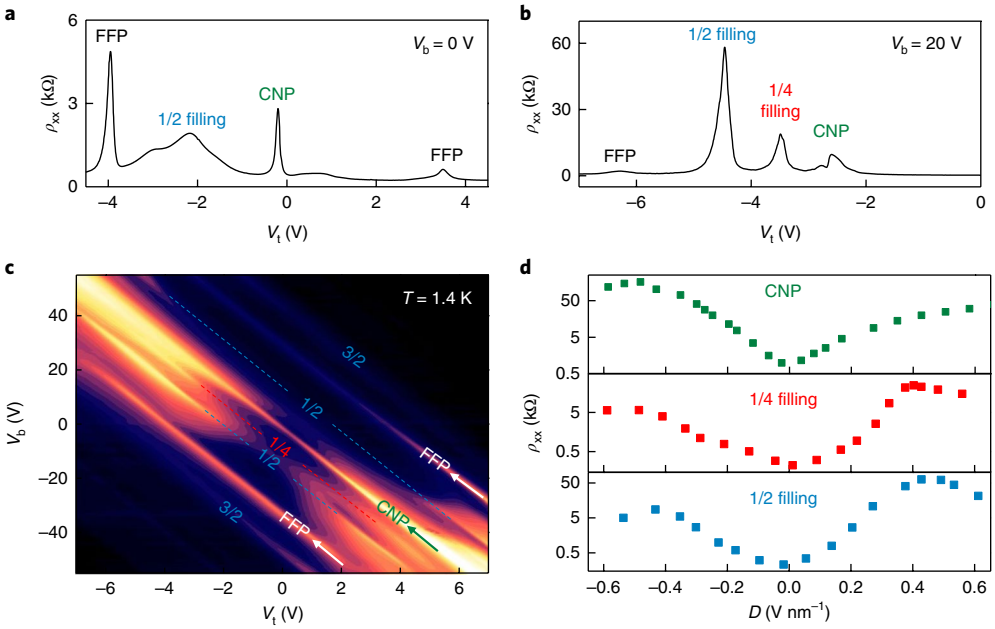

Fig. 2 | Transport of gate-tunable Mott state. a,**b**, Top-gate-dependent resistivity of the ABC-TLG/hBN moiré superlattice when $V_b = 0$ V (**a**) and 20 V (**b**), respectively. **c**, Colour plot of resistance as a function of V_t and V_b. The colour scale is from 10 Ω (dark) to 100 kΩ (bright) in a log scale. The highlighted straight lines correspond to the charge-neutrality point (CNP), 1/4 filling, 1/2 fillings, fully-filled point (FFP) and 3/2 fillings resistance peaks. **d**, Resistivity at the charge-neutral point (green), 1/4 filling in the hole side (red) and 1/2 filling in the hole side (blue) tuned by electric displacement D. The insulating behaviour at 1/4 and 1/2 fillings, corresponding to one and two charges per lattice site, provides the defining signature of a Mott insulator.

when the moiré minibands are completely filled. Such resistance peaks can arise from secondary Dirac points with monolayer graphene or fully gapped insulating states with bilayer or ABC-TLG[10–13,26]. Figure 2a presents a plot of the gate-dependent four-probe resistivity (ρ_{xx}) at 1.4 K in a near-zero-twist ABC-TLG/hBN heterostructure, where the top and bottom hBN thicknesses are 38 nm and 40 nm, respectively. For these measurements we fixed the bottom gate voltage (V_b) at 0 V, and swept the top gate voltage (V_t) from −4.5 to 4.5 V. In addition to a large resistance peak at the charge-neutral point at $V_t^0 = -0.2$ V, two extra prominent resistance peaks appear symmetrically around the charge-neutral point at gate voltages $V_t - V_t^0 = \pm 3.8$ V. These correspond to an electron and hole density of $n_{FFP} = 2.1 \times 10^{12}$ cm^{-2} based on the capacitance model using a top hBN thickness of 38 nm and an hBN vertical dielectric constant of 4. The secondary resistance peaks are similar to those observed in monolayer and bilayer graphene/hBN moiré superlattices. They arise from fully filled moiré superlattice minibands, and we denote them as fully filled points (FFP). The moiré superlattice period can be obtained by the relation $L_M = \sqrt{\frac{8}{\sqrt{3} n_{FFP}}} = 15$ nm. An independent and more accurate determination of n_{FFP} and the moiré wavelength through the Landau level fan diagram confirmed these results (see Supplementary Section II for details.) The emerging feature that distinguishes the ABC-TLG/hBN heterostructure is the extra prominent resistance maxima in the partially filled hole miniband, including a resistance peak close to 1/2 filling. This is in striking contrast to a typical band insulator (including the monolayer or bilayer graphene/hBN superlattice), where the resistance is close to a minimum value at 1/2 filling. Such a resistance peak close to 1/2 filling implies strongly correlated electronic states in the ABC-TLG/hBN heterostructure.

Further enhancement of the quantum correlation in electronic states can be achieved by suppressing the energy bandwidth of electronic bands. This can be realized in the ABC-TLG/hBN heterostructure through a vertical electrical field, which is known to induce a finite bandgap in ABC-TLG. Experimentally, we controlled the vertical electrical field strength and the carrier doping in the ABC-TLG/hBN heterostructure independently by varying both the top and bottom gate voltages[28]: the vertical displacement field across the ABC-TLG is set by $D = \frac{1}{2}(D_b + D_t)$ and the charge concentration is determined by $n = (D_b - D_t)/e$. Here, $D_b = +\varepsilon_b(V_b - V_b^0)/d_b$ and $D_t = -\varepsilon_t(V_t - V_t^0)/d_t$, where ε and d are the dielectric constant and thickness of the dielectric layers, respectively, and V_b^0 and V_t^0 are effective offset voltages caused by environment-induced carrier doping. Figure 2c shows a 2D plot of the ρ_{xx} value as a function of V_t and V_b. The resistivity peaks at the charge-neutral point, and fully filled points persist at all displacement fields. In particular, the resistivity at the charge-neutral point increases monotonically with the vertical displacement field strength, as shown in Fig. 2d, indicating an increased bandgap energy at the charge-neutral point. More strikingly, the resistivity peaks at partial filling become much sharper and more prominent at higher vertical displacement fields. Resistivity peaks can be clearly identified at 1/4 and 1/2 filling of the first hole miniband, and at 1/2 filling of the first electron miniband (dashed lines in Fig. 2c). The difference between the electron and hole minibands presumably arises from the electron–hole asymmetry present in ABC-TLG[4]. Figure 2b shows a horizontal line cut of Fig. 2c at $V_b = 20$ V. The prominent resistance peaks at 1/4 and 1/2 fillings of the hole miniband are very sharp, and they are comparable, or even more insulating than the charge-neutral point and fully filled points. The 1/4 and 1/2 filling states correspond to one electron and two electrons per superlattice unit cell, respectively, and this observation is the defining signature of a Mott insulator. Magnetotransport data show that the resistance peaks at 1/4 and 1/2 filling states also feature zero Hall carrier density, further indicating the existence of a gapped insulator (see Supplementary Section III for details). This Mott insulator in the ABC-TLG/hBN superlattice offers unprecedented control of the Mott states: the insulating states can be strongly modified in situ by changing the vertical electrical field, and the carrier doping can be gate-tuned through the whole Mott band so that we can change from one Mott insulating state to another.

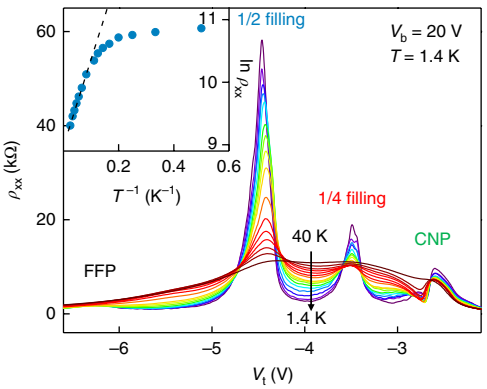

Fig. 3 | Temperature-dependent resistivity. Plot of ρ_{xx} at different top-gate voltages and fixed V_b of 20 V for temperatures ranging from 1.5 K to 40 K. The resistivity peaks at 1/2 filling and 1/4 filling exhibit typical insulating behaviour where the resistance increases with reduced temperature. Inset, the corresponding $\ln\rho_{xx}$ versus $1/T$ plot at 1/2 filling, where the estimated transport Mott gap is $\Delta_t = 2$ meV.

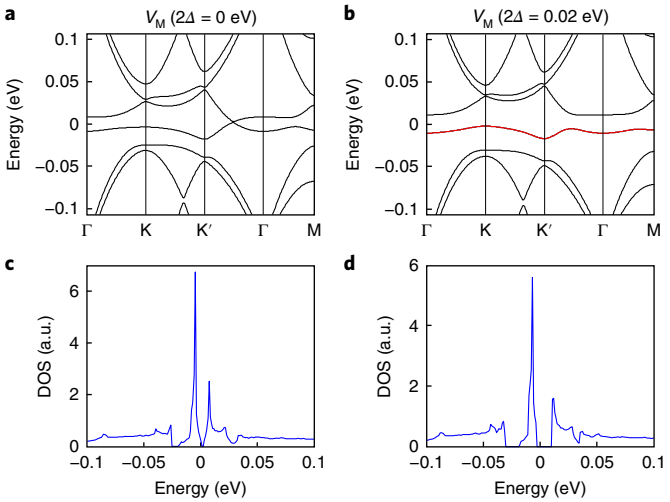

Fig. 4 | Single-particle band structure of ABC-TLG/hBN moiré superlattice. **a**,**b**, Energy dispersion of the two electron and hole minibands without (**a**) and with (**b**) a vertical electrical field, respectively. The vertical electrical field in **b** generates a potential difference of 20 meV between the top and bottom graphene layers. It leads to an isolated hole miniband with strongly suppressed bandwidth. The reduced electronic bandwidth relative to the Coulomb interaction enhances the electron correlation, and leads to the tunable Mott insulator states observed experimentally. **c**,**d**, Density of states (DOS) associated with the band structures in **a** and **b**, confirming the electron–hole asymmetry observed in our measurements. The bandgap at charge neutrality due to the vertical electric field isolates the fourfold degenerate superlattice flat band of the hole side.

To estimate the Mott gap of the insulating states, we measured the temperature dependence of the transport behaviour in the ABC-TLG/hBN heterostructure. Figure 3 shows a representative data set of resistivity versus temperature at $V_b = 20$ V. The resistivity peaks at 1/4 and 1/2 fillings exhibit typical insulating behaviour where the resistance increases with reduced temperature. The inset shows a plot of $\ln\rho_{xx}$ versus $1/T$ for the 1/2 filling point, from which we can estimate an 'effective transport gap' Δ_t of ~2 meV.

Next we examine theoretically the competition between the moiré miniband bandwidth (W) and the Coulomb repulsion energy (U) in the ABC-TLG/hBN heterostructure with an $L_M = 15$ nm moiré superlattice. The single-particle bandstructure of the heterostructure is described by the Hamiltonian $H = H_{ABC} + V_M$, where H_{ABC} is the ABC-TLG Hamiltonian under a weak vertical electrical field, and V_M describes the effective potential acting on ABC-TLG from the moiré superlattice. The low-energy electronic structure of the ABC-TLG can be captured by an effective two-component Hamiltonian in the K valley that describes hopping between the A atom in the top graphene layer and the C atom in the bottom graphene layer[4,5]:

$$H_{ABC} = \frac{v_0^3}{t_1^2}\begin{pmatrix} 0 & (\pi^+)^3 \\ \pi^3 & 0 \end{pmatrix} + \left(\frac{2v_0v_3p^2}{t_1} + t_2\right)\begin{pmatrix} 0 & 1 \\ 1 & 0 \end{pmatrix} + \left(\frac{2v_0v_4p^2}{t_1} - \Delta'\right)\begin{pmatrix} 1 & 0 \\ 0 & 1 \end{pmatrix} + \left(\frac{3v_0^2p^2}{t_1^2} - 1\right)\Delta''\begin{pmatrix} 1 & 0 \\ 0 & 1 \end{pmatrix} - \Delta\begin{pmatrix} 1 & 0 \\ 0 & -1 \end{pmatrix}$$

where $\pi = p_x + ip_y$, $\mathbf{p}$ is the electron momentum, 2Δ is the electron energy difference between the top and bottom layer due to the vertical electrical field $v_i \equiv \left(\frac{\sqrt{3}}{2}\right) a t_i/\hbar$, $a = 2.46$ Å is the carbon–carbon lattice constant, $\Delta' \approx 0.0122$ eV, $\Delta'' \approx -0.0095$ eV and t_0, t_1, t_2, t_3 and t_4 are tight binding parameters in ABC-TLG obtained from local density approximation (LDA) ab initio calculations with values of 2.62, 0.358, −0.0083, 0.293 and 0.144 eV, respectively. We consider that the encapsulated ABC-TLG forms a near-zero-twist moiré superlattice with the hBN on one side, for example, as a bottom hBN film. The ABC-TLG/hBN interaction in the K valley can be approximated by a potential of the form $V_M^{A/B}(\mathbf{r}) = 2C_{A/B}\mathrm{Re}[e^{i\varphi_{A/B}}f(\mathbf{r})]\begin{pmatrix} 1 & 0 \\ 0 & 0 \end{pmatrix}$ acting at the low energy site of the effective ABC-TLG in contact with the substrate[17], where $f(\mathbf{r}) = \sum_{j=1}^{6} e^{i\mathbf{q}_j\mathbf{r}}(1 + (-1)^j)/2$ and $\mathbf{q}_j$ are the six reciprocal lattice vectors of the triangular moiré superlattice with $|\mathbf{q}_j| = q_M \equiv \frac{4\pi}{\sqrt{3}L_M}$. The hBN layer periodically modulates the potential in the bottom-layer carbon atom whose magnitude and phase parameters are $C_A = -14.88$ meV and $\varphi_A = 50.19°$ (refs. [14,15]). We solve the Hamiltonian numerically by direct diagonalization with a momentum cutoff at $5q_M$. Figure 4a displays the energy dispersion of the two lowest electron and hole minibands in the ABC-TLG/hBN heterostructure without an electrical field. The first hole miniband has a bandwidth of $W \approx 20$ meV. On applying an external vertical displacement field of 0.4 V nm^{-1}, we generate a potential difference between the top and bottom layer of ABC-TLG of ~20 meV (ref. [5]). The calculated miniband dispersion for $2\Delta = 20$ meV is displayed in Fig. 4b. We observe that the first hole miniband is strongly suppressed by the vertical field and has $W \approx 13$ meV. In particular, the hole miniband is well separated from other bands by over 10 meV. The on-site Coulomb repulsion energy can be estimated by $U \approx \frac{e^2}{4\pi\varepsilon_0\varepsilon L_M}$. For $L_M = 15$ nm and an hBN dielectric constant $\varepsilon = 4$, U is ~25 meV, which is larger than the value of W. This dominating on-site Coulomb repulsion naturally leads to Mott insulator states in the isolated hole miniband when there are one or two holes per site, that is, at 1/4 and 1/2 filling of the band. The expected Mott gap ($\Delta_{Mott} \approx U - W$) should be ~10 meV, which agrees qualitatively with our experimental observation. More information about the minibands' electronic bandstructure and their evolution with the vertical electrical field are provided in Supplementary Section V.

The concept of engineering a moiré superlattice that exhibits correlated behaviour by controlling the competition between the kinetic and potential energy is generally applicable to many atomically thin 2D heterostructures, including twisted semiconducting transition metal dichalcogenide heterostructures, which feature a reasonably large electron mass. Such tunable Mott insulating states

in designed 2D heterostructures open up completely new ways to explore fascinating Mott physics. The doped Mott insulator in 2D heterostructures can provide a unique tunable quantum simulator of the Hubbard model[29]. The 2D heterostructures can also give rise to new correlated phenomena that are not present in conventional crystals, such as the correlations between the charge, spin and valley degrees of freedom, and the interplay between the Mott insulator and quantum Hall states under high magnetic field.

Data availability

The data that support the findings of this study are available from the corresponding authors upon reasonable request.

Received: 1 November 2018; Accepted: 27 November 2018;
Published online: 21 January 2019

References

1. Mott, N. F. The basis of the electron theory of metals, with special reference to the transition metals. *Proc. Phys. Soc. Lond. A* **62**, 416–422 (1949).
2. Imada, M., Fujimori, A. & Tokura, Y. Metal–insulator transitions. *Rev. Mod. Phys.* **70**, 1039–1263 (1998).
3. Lee, P. A., Nagaosa, N. & Wen, X. G. Doping a Mott insulator: physics of high-temperature superconductivity. *Rev. Mod. Phys.* **78**, 17–85 (2006).
4. Koshino, M. & McCann, E. Trigonal warping and Berry's phase $N\pi$ in ABC-stacked multilayer graphene. *Phys. Rev. B* **80**, 165409 (2009).
5. Zhang, F., Sahu, B., Min, H. K. & Macdonald, A. H. Band structure of ABC-stacked graphene trilayers. *Phys. Rev. B* **82**, 035409 (2010).
6. Bao, W. et al. Stacking-dependent band gap and quantum transport in trilayer graphene. *Nat. Phys.* **7**, 948–952 (2011).
7. Lui, C. H., Li, Z. Q., Mak, K. F., Cappelluti, E. & Heinz, T. F. Observation of an electrically tunable band gap in trilayer graphene. *Nat. Phys.* **7**, 944–947 (2011).
8. Zhang, L. Y., Zhang, Y., Camacho, J., Khodas, M. & Zaliznyak, I. The experimental observation of quantum Hall effect of l = 3 chiral quasiparticles in trilayer graphene. *Nat. Phys.* **7**, 953–957 (2011).
9. Yankowitz, M. et al. Emergence of superlattice Dirac points in graphene on hexagonal boron nitride. *Nat. Phys.* **8**, 382–386 (2012).
10. Dean, C. R. et al. Hofstadter's butterfly and the fractal quantum Hall effect in moiré superlattices. *Nature* **497**, 598–602 (2013).
11. Hunt, B. et al. Massive Dirac fermions and Hofstadter butterfly in a van der Waals heterostructure. *Science* **340**, 1427–1430 (2013).
12. Ponomarenko, L. A. et al. Cloning of Dirac fermions in graphene superlattices. *Nature* **497**, 594–597 (2013).
13. Wallbank, J. R., Patel, A. A., Mucha-Kruczynski, M., Geim, A. K. & Falko, V. I. Generic miniband structure of graphene on a hexagonal substrate. *Phys. Rev. B* **87**, 245408 (2013).
14. Jung, J., Raoux, A., Qiao, Z. & MacDonald, A. H. Ab initio theory of moiré superlattice bands in layered two dimensional materials. *Phys. Rev. B* **89**, 205414 (2014).
15. Jung, J., DaSilva, A. M., MacDonald, A. H. & Adam, S. A. Origin of band gaps in graphene on hexagonal boron nitride. *Nat. Commun.* **6**, 6308 (2015).
16. Geim, A. K. & Grigorieva, I. V. Van der Waals heterostructures. *Nature* **499**, 419–425 (2013).
17. Yang, W. et al. Epitaxial growth of single-domain graphene on hexagonal boron nitride. *Nat. Mater.* **12**, 792–797 (2013).
18. Shi, Z. et al. Gate-dependent pseudospin mixing in graphene/boron nitride moiré superlattices. *Nat. Phys.* **10**, 743–747 (2014).
19. Mak, K. F., Lee, C., Hone, J., Shan, J. & Heinz, T. F. Atomically thin MoS_2: a new direct-gap semiconductor. *Phys. Rev. Lett.* **105**, 136805 (2010).
20. Splendiani, A. et al. Emerging photoluminescence in monolayer MoS_2. *Nano. Lett.* **10**, 1271–1275 (2010).
21. Rivera, P. et al. Valley-polarized exciton dynamics in a 2D semiconductor heterostructure. *Science* **351**, 688–691 (2016).
22. Yu, H. Y., Wang, Y., Tong, Q. J., Xu, X. D. & Yao, W. Anomalous light cones and valley optical selection rules of interlayer excitons in twisted heterobilayers. *Phys. Rev. Lett.* **115**, 187002 (2015).
23. Wang, L. et al. One-dimensional electrical contact to a two-dimensional material. *Science* **342**, 614–617 (2013).
24. Novoselov, K. S. et al. Two-dimensional gas of massless Dirac fermions in graphene. *Nature* **438**, 197–200 (2005).
25. Zhang, Y. B., Tan, Y. W., Stormer, H. L. & Kim, P. Experimental observation of the quantum Hall effect and Berry's phase in graphene. *Nature* **438**, 201–204 (2005).
26. Lee, Y. et al. Competition between spontaneous symmetry breaking and single-particle gaps in trilayer graphene. *Nat. Commun.* **5**, 5656 (2014).
27. Ju, L. et al. Topological valley transport at bilayer graphene domain walls. *Nature* **520**, 650–655 (2015).
28. Zhang, Y. B. et al. Direct observation of a widely tunable bandgap in bilayer graphene. *Nature* **459**, 820–823 (2009).
29. Hubbard, J. Electron correlations in narrow energy bands. *Proc. R. Soc. Lond. A* **276**, 238–257 (1963).

Acknowledgements

The authors thank C. Jin, E. Regan, X. Lu, Y. Shan, S. Wu and G. Zhang for discussions and help with sample preparation. The trilayer graphene sample fabrication and experimental study was supported by the Office of Naval Research (award no. N00014-15-1-2651). The initial idea and proof-of-principle calculation of 2D flatband engineering was supported by an ARO MURI award (W911NF-15-1-0447). Part of the sample fabrication was conducted at the Nano-fabrication Laboratory at Fudan University. B.L.C. was supported by the Basic Science Research Program through the National Research Foundation of Korea (NRF) funded by the Ministry of Education (2018R1A6A1A06024977) and by grants NRF-2016R1A2B4010105 and NRF-2017R1D1A1B03035932. J.J. was supported by the Samsung Science and Technology Foundation under project no. SSTF-BA1802-06. Y.Z. acknowledges financial support from the National Key Research Program of China (grant nos. 2016YFA0300703 and 2018YFA0305600), the NSF of China (grant nos. U1732274, 11527805, 11425415 and 11421404), Shanghai Municipal Science and Technology Commission (grant no. 18JC1410300) and the Strategic Priority Research Program of the Chinese Academy of Sciences (grant no. XDB30000000). Z.S. is supported by the Program for Professor of Special Appointment (Eastern Scholar) at Shanghai Institutions of Higher Learning and the National Natural Science Foundation of China under grant no. 11574204. B.L., H.L. and Z.S. are supported by the National Key Research and Development Program of China (grant 2016YFA0302001) and National Natural Science Foundation of China (grants 11574204, 11774224). Growth of hBN crystals was supported by the Elemental Strategy Initiative conducted by the MEXT, Japan and JSPS KAKENHI grant no. JP15K21722. Part of the sample fabrication was conducted at Fudan Nano-fabrication Lab.

Author contributions

F.W. and Y.Z. supervised the project. G.C. fabricated samples and performed transport measurements. G.C., L.J., S.W., B.L., H.L. and Z.S. prepared trilayer graphene and performed near-field infrared and atomic force microscopy measurements. B.L.C. and J.J. calculated the band structures. K.W. and T.T. grew hBN single crystals. G.C., Y.Z. and F.W. analysed the data.

Competing interests

The authors declare no competing interests.

Additional information

Supplementary information is available for this paper at https://doi.org/10.1038/s41567-018-0387-2.

Reprints and permissions information is available at www.nature.com/reprints.

Correspondence and requests for materials should be addressed to Y.Z. or F.W.

Publisher's note: Springer Nature remains neutral with regard to jurisdictional claims in published maps and institutional affiliations.